Optical and Electrical Characterization of (002)-Preferentially Oriented *n*-ZnO/*p*-Si Heterostructure

B. Abdallah, S. Al-Khawaja*
Department of Physics, Atomic Energy Commission of Syria, P.O. Box 6091, Damascus, Syria

(Received January 28, 2015; revised version May 5, 2015; in final form June 1, 2015)

In this paper, preferentially oriented (002) ZnO thin films have been grown on Si (100) and glass substrates using radio frequency magnetron sputtering. The dependence of the quality of the ZnO thin films at different substrate temperatures on the growth is studied. A ZnO thin film with *c*-axis-oriented würtzite structure is obtained at a growth temperature from 200 to 400 °C. X-ray diffraction shows that the full width at half maximum θ–2θ of (002) ZnO/Si is located at approximately 34.42°, which is used to infer the grain size that is found to be 17 nm to 19.7 nm. The FWHM is 9.5° to 8° in rocking curve mode, from which the crystalline quality has been determined. The texture degree demonstrates the improvement in quality with the increase of substrate temperature, which is best at 400 °C. The band gap extracted by UV transmittance spectrum has been identified as 3.2 eV at 400 °C. The electrical characteristics via C–V and I–V measurements on the basis of the heterojunction thermal emission model confirm the domination of high-density grain boundary layer existing at the interface. The transport currents indicate to the presence of space-charge-limited current and trap-charge-limited current mechanisms.

DOI: 10.12693/APhysPolA.128.283
PACS: 47.15.gm, 66.70.Df, 68.60.–p

1. Introduction

Zinc oxide (ZnO) is a direct wide-band gap material of 3.37 eV, and exciton binding energy around 60 meV at room temperature. For this reason, ZnO is considered to have quite superior electronic properties over classical semiconductors like Si and GaAs, with its components being exuberantly existing in nature, inexpensive, non-toxic, very environmentally stable, highly conductive and transparent as well, with sensitivity in the ultraviolet region (UV). ZnO is thus useful as transparent electrode in solar cells [1], crystal display (LCD) [2], and light emitting diode (LED) [3]. Moreover, ZnO can be exploited in thin film transistors (TFT) [4, 5], gas sensor [6], laser diode and UV photodetector [7–10]. The common wide-band gap material usually used in electronic and photonic applications particularly as a transparent electrode is tin-doped indium oxide (ITO). However, we know that indium is costly and very expensive, due to rare materials, estimated to be 0.05–0.25 ppm [11]. If we compare it with that of ZnO which has 76 ppm, we find that this value is completely higher than indium in ITO. Moreover, ITO is a toxic material to both human body and environment. Therefore, ZnO is expected on the long run to replace ITO as the main material given the potential electronic and photonic implementations of which, such as transparent electrode in solar cells [12, 13], transparent conductor, piezoelectric transducer and surface acoustic wave device [14–16].

The increase in the ZnO conductivity can be realised by thermal treatment with hydrogen [17, 18] or by appropriate doping process [19]. ZnO belongs to the transparent conductive oxides group (TCO) and doping ZnO on the other hand, can be achieved by adding a small amount of group III elements (such as B, Al, In or Ga) or IV elements (such as Pb, Se), and various deposition techniques have been performed to prepare doped ZnO thin films [20, 21]. Among the preparation methods, magnetron sputtering has been the most widely utilized since it enables working at low temperatures and provides deposits of improved adhesion and higher density than other methods [22]. Most importantly, ZnO can be band-gap engineered by alloying it with MgO and CdO to increase and decrease its energy band gap respectively [23], so that its optoelectronic properties may be fiddled with. We have recently observed, thanks to high resolution transmission electron microscopy (HRTEM) images and selected area electron diffraction patterns, that the ZnO film deposited on AlN substrate exhibits an epitaxial growth that is strongly dependent on the crystalline quality of the AlN film [24]. Many authors have reported the fabrication of ZnO-based heterojunctions and studied their crystalline and electrical properties [25–27], and found that the latter rely significantly on both thermal conditions during preparation and on post annealing. Such treatment affects the grain boundaries of the ZnO film and potentially its interfacial states, donor concentration and consequently its barrier height. The objective of this article is thus to prepare *n*-ZnO/*p*-Si heterostructure with good crystalline quality, and investigate the optical and electrical behaviour of the metal–semiconductor (MS) interface for different substrate temperatures, and explore the conduction mechanism of the *n*–*p* heterostructure. Achieving high quality devices of such semiconducting material depends crucially on preparation conditions such as

*corresponding author; e-mail: pscientific@aec.org.sy

the plasma parameters and growth temperature which lead to improved film structural quality, and as a consequence influences the electrical and optical properties as we shall demonstrate. Aluminum has been chosen as the metal contact that forms the heterostructure of ZnO film; transmittance, current–voltage and capacitance voltage measurements are provided.

2. Experimental procedure

Zinc oxide films have been elaborated by RF magnetron sputtering using a PLASSYS setup with embedded micro balance for controlling the deposition thickness. The quality of the prepared films has been very sensitive to deposition parameters which have been, therefore, optimised in order to obtain highly oriented ZnO films. The ZnO films were deposited on p-type silicon wafers of (100) orientation with a resistivity of 50 Ω cm and on glass substrates. Prior to deposition, the substrates were ultrasonically cleaned in acetone and ethanol solution to eliminate any native oxide. However, SiO_2 layer could still be dominant as it is difficult to be completely removed and hence it might contribute to the ohmic resistance of the films at the interface. The zinc oxide target (purity 99.99%) diameter was 15 cm and 6 mm thick. The distance between the cathode and the substrate holder was 6 cm. The deposition chamber was pumped down to a base pressure of 2×10^{-7} Torr by a turbomolecular pump prior to the introduction of the argon gas for ZnO thin film production. The film thickness was fixed at 100 nm using *in situ* microbalance. The substrate holder temperature was varied from 200 °C to 400 °C at RF power of 600 W; all these conditions are summarised below.

Optimised preparation conditions and parameters of ZnO deposition are:

- RF power — 600 W,
- ZnO target of 99.99% purity,
- Gas flow — 11 sccm,
- temperature — 200 to 400 °C,
- pressure — 1 mTorr,
- film thickness — 100 nm

The crystallographic properties of the films were analysed by X-ray diffraction (XRD) using the Cu K_α (with $\lambda = 1.5405$ Å) radiation. Metallic contacts were made by depositing circular aluminum spots (area = 0.48 mm^2) on ZnO films, and electrical connections were made using the QuadTech low voltage chip component test fixture onto ZnO films for the top electrode and to p-silicon as the bottom electrode.

The optical characteristics were examined using a UV-vis Shimadzu UV-310PC Spectrophotometer to measure the transmittance of films. The electrical properties (C–V and I–V) on the other hand, were measured using the HP 4192A impedance analyser, QuadTech 1920 LCR meter and Keithley 237 source measure unit.

3. Results and discussion

3.1. Structural and morphological properties

Figure 1a shows the XRD pattern of n-ZnO/p-Si samples deposited at several temperatures from 200 °C to 400 °C at a pressure of 1 mTorr. We observe only one strong peak at $2\theta \approx 34.4°$, which is attributed to the (002) line of the hexagonal ZnO würtzite phase [28]. All the sputtered ZnO films are highly textured, with the c-axis perpendicular to the substrate surface.

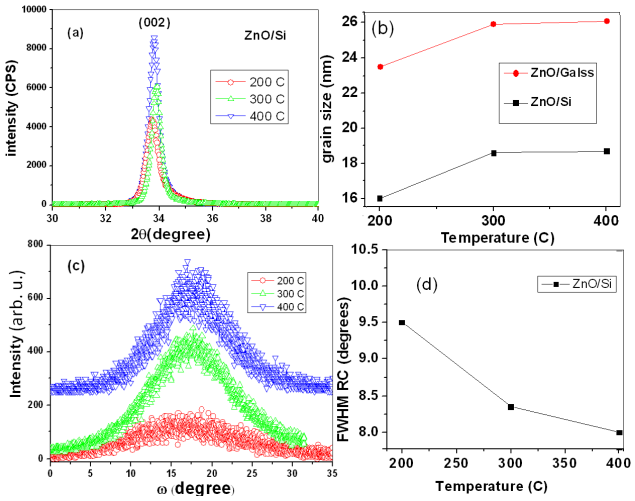

Fig. 1. (a) XRD patterns of ZnO films at 200, 300 and 400 °C temperature, (b) grain size, (c) rocking curve patterns and (d) FWHM for rocking curve as a function of temperature.

The mean grain size d is obtained by the Scherrer formula [29], $d = 0.94\lambda/(B\cos\theta)$, where λ, θ and B are the X-ray wavelength (1.54 Å), the Bragg diffraction angle, and the line width at half maximum of the peak, respectively.

The rocking curve spectra show an improvement in the crystallinity of films, while its FWHM decreases. Further, Fig. 1b demonstrates that the increase of substrate temperature leads to a slight grain size increase from 16 nm to 19.7 nm for ZnO/Si and form 23.5 nm to 26 nm for ZnO/glass with temperature within 200 to 400 °C. The improvement in the quality is verified by rocking curve technique (Fig. 1c and d), where the FWHM decreases from 9.5° to 8° with temperature. The XRD spectrum reveals a better crystalline quality for the 400 °C film. Moreover, the peak intensity is observed to increase and the grain size is the highest at such temperature. This is consistent with previously reported results about the crystalline property which has been observed through the profile going to the film surface of ZnO, with very limited grain boundaries observed by HRTEM [19].

3.2. Optical properties

Figure 2a represents the optical transmittance of ZnO films deposited at 600 W of sputter power as a function of wavelength. The optical transmittance provides useful information about the optical band gap of the semiconductor. The absorption coefficient of a thin layer is expressed, as an approximation, by the following formula:

$$\alpha = A(h\nu - E_{\mathrm{g}})^{p}, \tag{1}$$

which is valid for energies $h\nu$ not exceedingly high, where A is a constant, $h\nu$ is the photon energy, E_{g} is the band gap and p is an exponent which provides information about the nature of the optical transitions between the valence and conduction bands; the value of p is 0.5 for allowed direct transitions in ZnO. The optical band gap E_{g} of ZnO thin films can be deduced from Fig. 2b, which demonstrates a plot of α^2 versus $h\nu$ that is expected to be linear within the approximation limit of Eq. (1). One may extend the linear part of α^2 as a straight asymptotic line that intercepts the horizontal axis $\alpha^2 = 0$) yielding E_{g} from $h\nu$ value [30, 31].

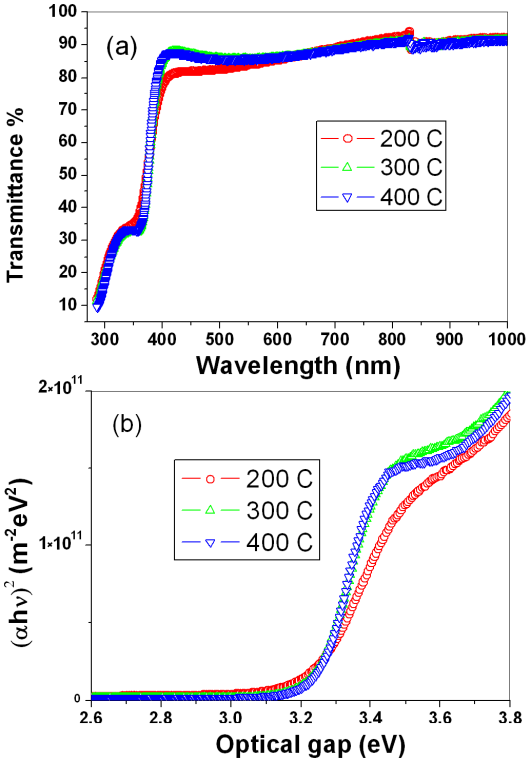

Fig. 2. (a) Optical transmittance spectra versus wavelength, (b) variations of α^2 as a function of photon energy for films at different temperatures.

It has been observed that the average transmittance of samples in the visible range rises from 80% to 92% as the temperature increases. Figure 2a shows the transmittance spectra of ZnO thin films obtained.

The optical transmittance spectra of ZnO films prepared at different temperatures are depicted in Fig. 2a. A pronounced absorption peak of the free exciton is clearly located at 3.16, 3.19, and 3.2 eV for 200, 300, and 400 °C, respectively. In addition, the spectral curves show a unique phenomenon, namely the rise of a shoulder in the wavelength range between 300 and 380 nm. Chang et al. [32] and Leanddas et al. [33] pointed out that the emergence of a shoulder for all ZnO films is probably caused by electron trapping phenomena in the wavelength range of 230–350 nm. The largest value of the optical band gap (3.2 eV) is probably related to the nanoscopic size of crystallites [34].

3.3. Electrical characteristics

The I–V characteristics under forward bias condition of three samples prepared at substrate temperatures 200, 300, and 400 °C, respectively, at 600 W of power are shown in Fig. 3. The curves reveal that the current transport mechanism is dominated mainly by the grain boundary existing within ZnO. Electrons in p-region are injected to the interface by means of tunnelling and traverse the grain boundary barrier by thermal emission when applying a reverse bias.

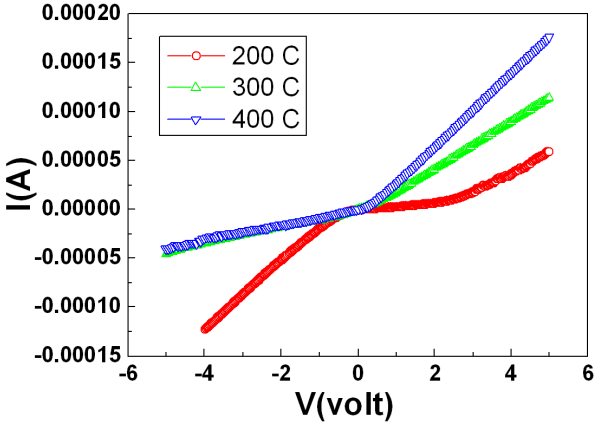

Fig. 3. The measured I–V curves for ZnO/Si at different substrate temperatures.

Adopting the conventional heterojunction thermal emission model [35, 36], the I–V characteristics can be expressed as

$$I = I_{\mathrm{s}}\left[\exp\left(\frac{qV - IR_{\mathrm{s}}}{nkT}\right)\right] \tag{2}$$

for $V > 3kT/q$, where q is the electron charge, k — the Boltzmann constant, T — the absolute temperature, V — the applied voltage, R_{s} — the series resistance, n — the ideality factor and I_{s} — the saturation current, which is written as

$$I_{\mathrm{s}} = A^{*}ST^{2}\exp(-q\phi_{\mathrm{b}}/kT), \tag{3}$$

where $A*$ is the effective Richardson constant, S — the area of the MS junction, and $q\phi_{\mathrm{b}}$ — the barrier height in units of eV. Plotting the I–V characteristics on semilog scale as in Fig. 4, it is notable that as the voltage gets higher, the curves become more deviated from exponential behaviour manifesting the effect of the series resistance.

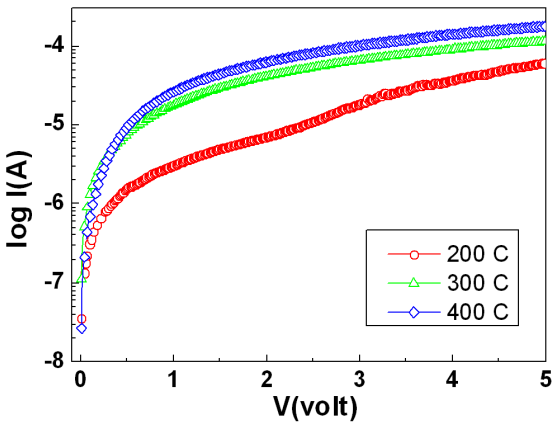

Fig. 4. $\log I$–V characteristics for ZnO/Si at different temperatures.

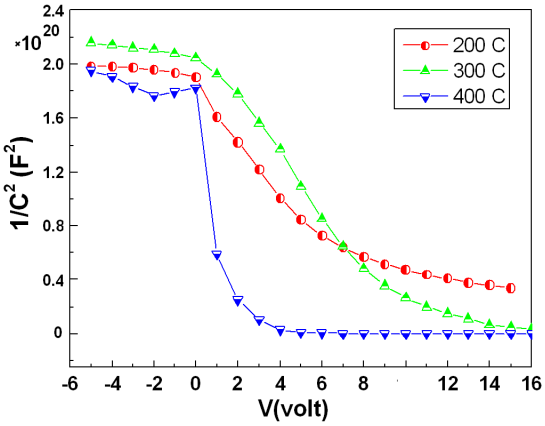

Fig. 5. Inverse of the square capacitance versus bias voltage of the ZnO heterostructure measured at 100 kHz.

The curves demonstrate relatively large values of R_s, which was estimated to be 12.6 kΩ at 400 °C indicating clearly to high ohmic contact of the junction due to interfacial oxide layer. R_s is calculated from the linear part of $\log I$ versus V (Fig. 4). Once the saturation current I_s is known, the barrier height can be determined accordingly (since $A* = 32$ A cm^{-2} K^{-2} for ZnO) [36]. An extrapolation of I versus V curve can be performed, and a straight line intercept of $\log I$ at $V = 0$ gives the values of I_s for both samples; from Fig. 4 I_s is found to be 3.5×10^{-8}, 1.1×10^{-7}, and 4×10^{-7} A at 200, 300, and 400 °C. This is in agreement with other reports which indicate to saturation current increase as the substrate temperature gets higher. Taking into consideration S to be 48×10^{-4} cm^2, the barrier height ϕ_b can thus be determined from Eq. (3) such as

$$\phi_\mathrm{b} = \frac{kT}{q} \ln\left(\frac{SA^*T^2}{I_\mathrm{s}}\right) \tag{4}$$

and found to be 0.31, 1.32 and 1.50 eV for the films at 200, 300, and 400 °C, respectively. The highest value of the barrier height as notable belongs to the junction at 400 °C.

Capacitance measurements have been performed on n-ZnO/p-Si samples at a functional frequency of 100 kHz with AC oscillation level set to 25 mV under forward and reverse DC bias voltage swept between −20 and 20 V (see Fig. 5). In the depletion region, one can use the following relation which gives the ionized donor concentration [36], that is:

$$\frac{1}{C^2} = \frac{2\left(V_\mathrm{bi} - V - \frac{kT}{q}\right)}{q\varepsilon_\mathrm{s}\varepsilon_0 S^2 N_\mathrm{d}}. \tag{5}$$

Here, ε_s is the permittivity of ZnO (≈8.5), ε_0 is the dielectric constant of vacuum, S — the junction area, V is the reverse-bias voltage, and N_d is the concentration of ionized donors in the depleted region which is found from differential capacitance voltage form such as

$$N_\mathrm{d} = \frac{2}{q\varepsilon_\mathrm{s}\varepsilon_0 S^2} \frac{1}{\mathrm{d}\left(C^{-2}\right)/\mathrm{d}V}. \tag{6}$$

Plotting $1/C^2$ versus V yields $\mathrm{d}(C^{-2})/\mathrm{d}V$ from the slope of the curves in the linear region, from which N_d is found to be 3.51×10^{16}, 3.55×10^{16} and 5.40×10^{15} cm^{-3} at 200, 300, and 400 °C, respectively. Our results are in accordance with the Chaabouni et al. findings (Ref. [27]) who concluded that ZnO/Si structures deposited by RF magnetron sputtering in a wider substrate temperature range between 25–400 °C have potential application as antireflectors in the UV region. Their electrical characteristics provide good support to interface homogeneity using the thermal emission model. Nonetheless, the data obtained in this paper demonstrate further that ZnO/Si films possess high transmittance (92%) for optimized power and substrate temperature concomitant with improvement to film's quality i.e., large grain size. This resulted also in improvement in the I–V characteristics of the films. From the electrical measurements we believe that the grain boundary at the interface plays a role in controlling charge carriers transport within the films, with larger saturation current and barrier height at higher temperature, but this needs further measurement techniques to be conclusive. The responsible current mechanisms are both the space-charge (SCLC) and trap-charge (TCLC) limited as deduced from fitting the I–V curves.

The built-in voltage V_bi which describes the electrostatic potential between the metal contact and the semiconducting ZnO layer can also be estimated from extension of the slopes of linear regions which intercept the voltage axis of C^{-2}–V curves. V_bi is equal to 1.6 eV for the junction at 400 °C which is the lowest in comparison to other samples.

In order to examine the transport mechanism, the current–voltage characteristics were plotted in double logarithmic scale as in Fig. 6. One can observe three regions of different slopes marking the curves that can be analysed employing the $I = aV^m$ relation where a and m are constants. Two regions depicted as SCLC in Fig. 6 refer to the existence of space-charge-limited current mechanism for which m was found to be 2.03 and 2.17,

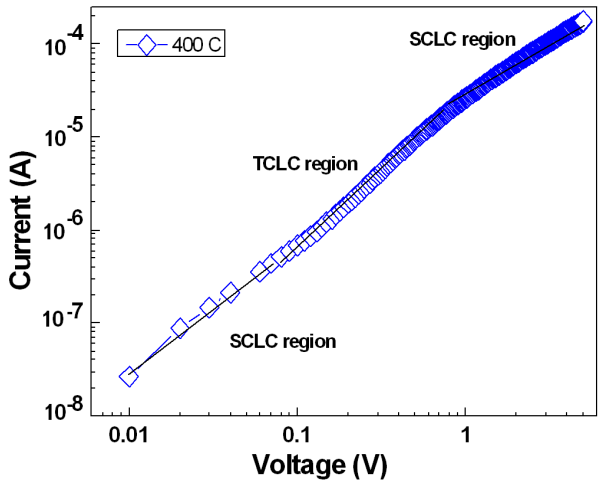

Fig. 6. The $I-V$ characteristics of ZnO/Si heterostructure on double logarithmic scale.

respectively. The region in the middle is characterised by the value 3.01 which indicates to trap-charge-limited mechanism referred to as TCLC in the plot.

4. Summary

Highly transparent and preferentially oriented ZnO films onto glass and Si have been prepared at different substrate temperatures using the RF magnetron sputtering technique. A systematic study of the influence of temperature on the physical properties of ZnO thin films has been carried out. X-ray diffraction analysis indicates that the films exhibited preferential orientation (002). The optimised sputtering power, substrate temperature and decreased argon gas pressure lead to the enlargement in the grain size and improvement in the crystalline quality as illustrated by X-ray rocking curves. The optical spectra emphasized that ZnO films showed high transmittance (92%) in the visible region. The dependence of the film quality on temperature is studied, and ZnO thin films with a *c*-axis orientated wurtzite structure are obtained. The strong UV band emission with a weak deep defect emission demonstrates that the ZnO thin films are stoichiometric. These conditions can be considered optimal to produce a good ZnO suitable for use as transparent electrode for optoelectronic devices. Electrical measurements on the metal–semiconductor heterostructure revealed that the current mechanism is dominated by grain boundary and trap charges layer at the ZnO interface. Series resistance, donor concentration and barrier height have been identified from I–V and C–V characteristics.

Acknowledgments

The authors would like to thank Prof. I. Othman the Director General of the Atomic Energy Commission of Syria for supporting this project, Drs. M. Saad and A. Kassis for using their facilities.

References

[1] Z.A. Wang, J.B. Chu, H.B. Zhu, Z. Sun, Y.W. Chen, S.M. Huang, *Solid State Electron.* **53**, 1149 (2009).

[2] B.Y. Oh, M.C. Jeong, T.H. Moon, W. Lee, J.M. Myoung, J.Y. Hwang, D.S. Seo, *J. Appl. Phys.* **99**, 124505 (2006).

[3] S.J. Pearton, W.T. Lim, J.S. Wright, L.C. Tien, H.S. Kim, D.P. Norton, H.T. Wang, B.S. Kang, F. Ren, J. Jun, J. Lin, A. Osinsky, *J. Electron. Mater.* **37**, 1426 (2008).

[4] R.L. Hoffman, B.J. Norris, J.F. Wager, *Appl. Phys. Lett.* **82**, 733 (2003).

[5] J. Zhu, H. Chen, G. Saraf, Z. Duan, Y. Lu, S.T. Hsu, *J. Electron. Mater.* **37**, 1237 (2008).

[6] V.R. Shinde, T.P. Gujar, C.D. Lokhande, *Sens. Actuat. B* **123**, 701 (2007).

[7] P.K. Basu, P. Battacharyya, N. Saha, H. Saha, S. Basu, *Sens. Actuat. B* **133**, 357 (2008).

[8] P.P. Sahay, R.K. Nath, *Sens. Actuat. B* **134**, 654 (2008).

[9] P.S. Cho, K.W. Kim, J.H. Lee, *J. Electroceram.* **17**, 975 (2006).

[10] Z. Bi, J.W. Zhang, X.M. Bian, D. Wang, X. Zhang, W.F. Zhang, X. Hou, *J. Electron. Mater.* **37**, 760 (2008).

[11] M.A. Green, *Prog. Photovolt. Res. Appl.* **17**, 347 (2009).

[12] S. Fay, S. Dubail, U. Kroll, J. Meier, Y. Zeigler, A. Shah, in: *Proc. 16th Photovoltaic Solar Energy Conf.*, Ed. H. Scheer, Taylor and Francis, Glasgow 2000, p. 362.

[13] K. Kushiya, M. Ohshita, I. Hara, Y. Tanaka, B. Sang, Y. Nagoya, M. Tachiyuki, O.'Yamase, *En. Mater. Sol. Cells.* **75**, 171 (2003).

[14] D.C. Look, *Mater. Sci. Eng. B* **80**, 383 (2001).

[15] A.B. Djurisic, Y. Chan, E.H. Li, *Mater. Sci. Eng. R* **38**, 237 (2002).

[16] S. Bensmaine, L. Le Brizoual, O. Elmazria, B. Assouar, B. Benyoucef, *J. Electron Dev.* **5**, 104 (2007).

[17] J.H. Lee, K.H. Ko, B.O. Park, *J. Cryst. Growth* **247**, 119 (2003).

[18] P. Nunes, E. Fortunato, R. Martins, *Int. J. Inorg. Mater.* **3**, 1125 (2001).

[19] S. Rahmane, M.A. Djouadi, M.S. Aida, N. Barreau, B. Abdallah, N. Hadj Zoubir, *Thin Solid Films* **519**, 5 (2010).

[20] J.H. Lee, B.O. Park, *Thin Solid Films* **426**, 94 (2003).

[21] V. Musat, B. Teixeira, E. Fortunato, R.C.C. Monteiro, P. Villarinho, *Surf. Coat. Technol.* **180–181**, 659 (2004).

[22] S. Al-Khawaja, B. Abdallah, S. Abou Shaker, M. Kakhia, *Composite Interfaces* **22**, 221 (2014).

[23] C. Jagadish, J. Peatron, *Zinc Oxide Bulk, Thin Films and Nanostructures Processing: Properties and Applications*, Elsevier, Amsterdam 2006.

[24] S. Rahmane, B. Abdallah, A. Soussou, E. Gautron, P.-Y. Jouan, L. Le Brizoual, N. Barreau, A. Soltani, M.A. Djouadi, *Phys. Status Solidi. A* **1–5**, 1604 (2010).

[25] X.Y. Peng, M. Sajjad, J. Chu, B.Q. Yang, P.X. Feng, *Appl. Surf. Sci.* **257**, 4795 (2011).

[26] L.J. Mandalapu, F.X. Xiu, Z. Yang, J.L. Liu, *J. Appl. Phys.* **102**, 023716 (2007).

[27] F. Chaabouni, M. Abaab, B. Rezig, *Superlatt. Microstruct.* **39**, 171 (2006).

[28] C. Messaoudi, D. Sayah, M. Abd-Lefdil, *Phys. Status Solidi A* **151**, 93 (1995).

[29] P. Scherrer, *Nachr. Ges. Wiss. Göttingen* **26**, 98 (1918).

[30] A.E. Rakhshani, *Appl. Phys. A* **92**, 413 (2008).

[31] M. Bouderbala, S. Hamzaoui, B. Amrani, A.H. Reshak, M. Adnane, T. Sahraoui, M. Zerdali, *Physica B Condens. Matter* **403**, 3326 (2008).

[32] H.J. Chang, C.Z. Lu, Y. Wang, C.S. Son, S.I. Kim, Y.H. Kim, I.H. Choi, *J. Korean Phys. Soc.* **45**, 959 (2004).

[33] Leanddas Nurdiwijayanto, Bambang Sunendar Purwasasmita, *J. Mater. Sci. Eng.* **11**, 1 (2010).

[34] G.G. Valle, P. Hammer, S.H. Pulcinelli, C.V. Santilli, *Europ. Ceram. Soc.* **24**, 1009 (2004).

[35] S.M. Sze, *Semiconductor Devices, Physics and Technology*, Wiley, USA 1985.

[36] D.K. Schroder, *Semiconductor Material and Device Characterization*, Wiley, USA 1990.